

Efficiency improvements of x-ray simulations in EGSnrc user-codes using bremsstrahlung cross-section enhancement (BCSE)

E. S. M. Ali^{a)} and D. W. O. Rogers^{b)}

Ottawa-Carleton Institute of Physics, Carleton University, Ottawa, K1S 5B6, Canada

(Received 30 September 2006; revised 4 April 2007; accepted for publication 5 April 2007; published 21 May 2007)

This paper presents the implementation of the bremsstrahlung cross-section enhancement (BCSE) variance-reduction technique into the EGSnrc/BEAMnrc system. BCSE makes the simulation of x-ray production from bremsstrahlung targets more efficient; it does so by artificially making the rare event of bremsstrahlung emission more abundant, which increases the number of statistically-independent photons that contribute to reducing the variance of the quantity of interest without increasing the CPU time appreciably. BCSE does not perturb the charged-particle transport in EGSnrc and it is made compatible with all other variance-reduction techniques already used in EGSnrc and BEAMnrc, including range rejection, uniform bremsstrahlung splitting, and directional bremsstrahlung splitting. When optimally combining BCSE with splitting to simulate typical situations of interest in medical physics research and in clinical practice, efficiencies can be up to five orders of magnitude larger than those obtained with analog simulations, and up to a full order of magnitude larger than those obtained with optimized splitting alone (which is the state-of-the-art of the EGSnrc/BEAMnrc system before this study was carried out). This study recommends that BCSE be combined with the existing splitting techniques for all EGSnrc/BEAMnrc simulations that involve bremsstrahlung targets, both in the kilovoltage and megavoltage range. Optimum cross-section enhancement factors for typical situations in diagnostic x-ray imaging and in radiotherapy are recommended, along with an easy algorithm for simulation optimization. © 2007 American Association of Physicists in Medicine. [DOI: [10.1118/1.2736778](https://doi.org/10.1118/1.2736778)]

I. INTRODUCTION

The efficiency ε of a Monte Carlo simulation is defined as

$$\varepsilon = \frac{1}{Ts^2}, \quad (1)$$

where T is the simulation CPU time and s^2 is an estimate of the statistical variance of the quantity of interest. According to this definition of simulation efficiency, analog Monte Carlo simulations involving bremsstrahlung targets operating in the kilovoltage range are very inefficient. This is because the probability of bremsstrahlung emission from electrons decelerating in the target material is very small, which means that most of the CPU time will be consumed in tracking electrons to a stop without their giving off any photons. We performed a Monte Carlo study in which a stream of monoenergetic electrons impinges onto a thick bremsstrahlung target, and the total number of bremsstrahlung events is counted and averaged over the total number of histories. Figure 1 shows the results for both tungsten and molybdenum targets. It can be seen that, on average, the probability of emission of a bremsstrahlung photon per incident electron is less than 10% for tungsten in the diagnostic range (around 100 keV) and less than 0.5% for molybdenum in the mammography range (around 20 keV). Even in the range of orthovoltage tubes (160–250 keV), the probability still does not exceed 20%.

To overcome this inefficiency of analog Monte Carlo simulation of bremsstrahlung targets, radiation transport Monte Carlo codes based on ETRAN¹ and PENELOPE^{2,3} have

included an option to enhance the production of bremsstrahlung photons and characteristic radiation if desired (called interaction forcing). However, to the authors' knowledge, there have not been any studies that optimized the use of this option or quantified the efficiency gains from implementing it in typical situations of interest in the medical physics field. In addition, the EGSnrc⁴/BEAMnrc⁵ system does not have this option because the system has been used mainly for simulation of medical linear accelerators where copious bremsstrahlung photons are emitted per incident charged particles, and no appreciable efficiency gains were expected from enhancing the bremsstrahlung cross section in the megavoltage range. This study both implements the bremsstrahlung cross section enhancement (BCSE) option into the EGSnrc/BEAMnrc system, and quantifies the associated efficiency gains from using it in typical situations of interest in diagnostic x-ray imaging and in radiotherapy.

The basic idea of the BCSE technique is to scale up the bremsstrahlung production cross section by a factor f_{enh} everywhere in the target material; then some aspects of the simulation are re-worked to keep the results unbiased. Such aspects include reducing the weight of the resulting bremsstrahlung photons in the target material by a factor of $1/f_{\text{enh}}$, and randomly decrementing the energy of the charged particle once every f_{enh} times of bremsstrahlung emission. In other words, the energy of the charged particle is *not* decremented every time a reduced-weight bremsstrahlung photon is emitted in the target material. This ensures that there is no bias that produces more photons near the target surface and disturbs the various features of the x-ray tube output (such as

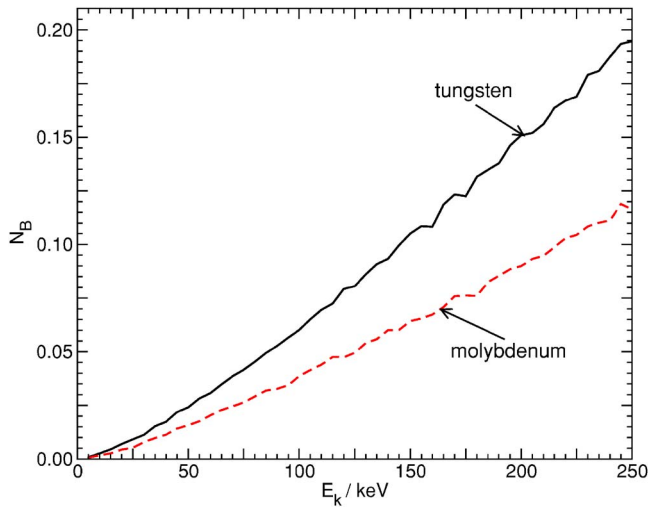


FIG. 1. The average number of bremsstrahlung photons N_B emitted by an electron slowing down from kinetic energy E_k to 1 keV inside thick tungsten and molybdenum targets, as a function of the initial electron kinetic energy E_k . The kinetic energy range shown covers that for mammography, diagnostic, and orthovoltage applications. The graph shows that bremsstrahlung emission is a rare event in the kilovoltage range, and this is the key to the efficiency gains obtained when the bremsstrahlung cross section is artificially enhanced.

the heel effect or the energy spectrum). It also ensures that the charged particle follows the same path it would have followed without BCSE; the only difference is that it gives off more reduced-weight bremsstrahlung photons everywhere (not only close to the surface). Generation of those statistically-independent extra photons reduces the fractional CPU time spent in tracking the charged particles, and hence increases the simulation efficiency. The benchmarking section in this study will unequivocally confirm that BCSE is a true variance-reduction technique and that it does not introduce any bias into the simulation.

EGSnrc is a widely-used Monte Carlo system for radiation transport. It started as a high-energy physics tool,⁶ but over the years many features have been added to accurately model the low-energy physics of photon and electron transport,^{7,8} and to use the state-of-the-art photon and electron cross sections.^{9–11} This makes the user-codes of the EGSnrc system, particularly BEAMnrc, ideally suitable for accurate simulation of kilovoltage x-ray sources. Such accurate simulations are essential for better assessment of image quality in diagnostic x-ray imaging, for better evaluation of patient entrance absorbed dose, and for better regulation of diagnostic and radiotherapy practice standards.¹² Studies simulating kilovoltage x-ray sources using EGSnrc (and its predecessors) have often been reported in the literature.^{12–18} Recently, miniature brachytherapy electronic x-ray sources have been simulated¹⁹ using BrachyDose,²⁰ a newly-developed EGSnrc user-code.

To improve the photon beam simulation efficiency in EGSnrc/BEAMnrc for bremsstrahlung targets, two variance-reduction techniques were made available in the system: uniform bremsstrahlung splitting (UBS) and directional bremsstrahlung splitting (DBS). UBS was introduced in the

original EGS4²¹/BEAM²² system. In UBS, after a bremsstrahlung photon is generated, it is split into N_{split} (a user-defined value) photons, each with a reduced weight of $1/N_{\text{split}}$, and then the N_{split} photons are tracked in all directions. UBS works best in 4π -geometry simulations (e.g., brachytherapy) because all the tracked split photons contribute to the scored quantity (e.g., dose to voxels). On the other hand, DBS²³ was introduced more recently into BEAMnrc. The basic concept of splitting in DBS is the same as in UBS. However, in DBS, only the split photons that are directed towards the field of interest are tracked, while Russian Roulette is played with the ones directed away from the field of interest. DBS works best in directional-geometry simulations (e.g., diagnostic tubes and medical linear accelerators) because the field of interest subtends a small solid angle, and tracking only the photons directed towards that small solid angle substantially reduces the simulation time.

Despite the large efficiency gains reported with UBS and DBS when they are optimized,^{23,24} there remain four issues. (1) Both splitting techniques will not come into play until the rare event of bremsstrahlung production happens in the first place. (2) EGSnrc uses a history-by-history statistical estimator²⁵ for the uncertainty on the scored quantity, which takes into account correlation between scored particles arising from the same incident particles. Since all N_{split} photons are correlated, efficiency gains saturate then drop once these correlated particles start falling into the same scoring zone or voxel.²⁶ (3) The large efficiency gains when using DBS are achieved for small field sizes (pinhole geometry for example),²⁴ but these gains decrease dramatically as the fields of interest get larger (e.g., a 40×40 cm² diagnostic field). (4) The only currently available variance-reduction technique in EGSnrc for 4π geometry is UBS, whose efficiency gains are not as impressive as those for DBS, and boosting them is very desirable. Combining BCSE with UBS/DBS alleviates the limitations caused by the four issues discussed above because BCSE will reduce the number of histories that do not generate bremsstrahlung photons, it will create more statistically-independent photons that push the efficiency gains of UBS and DBS further, and it will work equally well for small field sizes, large field sizes, and 4π geometry.

Although the main scope of the BCSE technique is the kilovoltage range, where bremsstrahlung production is rarest, its implementation in this study is made for the entire energy range. Both electron and positron bremsstrahlung emission is dealt with, and the term *charged particle* applies to both electrons and positrons.

II. IMPLEMENTING BCSE INTO EGSnrc/BEAMnrc

A. Enhancing the bremsstrahlung cross section

In EGSnrc, cross sections and other data are read from an input data file at the beginning of the simulation.⁴ For electron cross sections, the input data file includes the total discrete interaction cross section $\sigma_{\text{total_original}}$, and the branching ratio $B_{\text{brem_original}}$ for the fraction of discrete interactions that

are bremsstrahlung events. To enhance the bremsstrahlung cross section for a user-requested medium (typically the bremsstrahlung target, but it can be any other medium in the geometry) by a user-requested enhancement factor f_{enh} , the bremsstrahlung cross section is scaled to $\sigma_{\text{brem_enhanced}}$ and the total cross section and the bremsstrahlung branching ratio are adjusted to their new values $\sigma_{\text{total_new}}$ and $B_{\text{brem_new}}$ as follows:

$$\begin{aligned}\sigma_{\text{Moller}} &= \sigma_{\text{total_original}}(1 - B_{\text{brem_original}}), \\ \sigma_{\text{brem_enhanced}} &= \sigma_{\text{total_original}}B_{\text{brem_original}}f_{\text{enh}}, \\ \sigma_{\text{total_new}} &= \sigma_{\text{Moller}} + \sigma_{\text{brem_enhanced}}, \\ B_{\text{brem_new}} &= \sigma_{\text{brem_enhanced}} / \sigma_{\text{total_new}},\end{aligned}\quad (2)$$

where σ_{Moller} is the discrete electron-electron inelastic-scattering cross section. The two parameters $esig_e$ and $esig_max$, which are used in rejection sampling during the electron transport in EGSnrc, are also adjusted using the new total cross section $\sigma_{\text{total_new}}$ ($esig_e$ and $esig_max$ are the maximum electron cross section per unit restricted stopping power for the enhanced medium and for all media, respectively). For positrons, in addition to the quantities mentioned above for electrons, the input data file includes a second branching ratio, $B_{(\text{brem+Bhabha})_original}$, for the fraction of discrete interactions that are either bremsstrahlung or Bhabha events. The bremsstrahlung cross-section enhancement for positrons proceeds as follows:

$$\begin{aligned}\sigma_{\text{annih+Bhabha}} &= \sigma_{\text{total_original}}(1 - B_{\text{brem_original}}), \\ \sigma_{\text{Bhabha}} &= \sigma_{\text{total_original}}(B_{(\text{brem+Bhabha})_original} - B_{\text{brem_original}}), \\ \sigma_{\text{brem_enhanced}} &= \sigma_{\text{total_original}}B_{\text{brem_original}}f_{\text{enh}}, \\ \sigma_{\text{total_new}} &= \sigma_{\text{annih+Bhabha}} + \sigma_{\text{brem_enhanced}}, \\ B_{\text{brem_new}} &= \sigma_{\text{brem_enhanced}} / \sigma_{\text{total_new}}, \\ B_{(\text{brem+Bhabha})_new} &= (\sigma_{\text{brem_enhanced}} + \sigma_{\text{Bhabha}}) / \sigma_{\text{total_new}},\end{aligned}\quad (3)$$

where σ_{Bhabha} is the discrete positron-electron inelastic-scattering cross section and σ_{annih} is the discrete positron-electron annihilation cross section. As done for electrons, $psig_e$ and $psig_max$ are then adjusted using the new total cross section $\sigma_{\text{total_new}}$ ($psig_e$ and $psig_max$ are the maximum positron cross section per unit restricted stopping power for the enhanced medium and for all media, respectively). To avoid enhancing the bremsstrahlung cross section outside the target when other components of the system are made of the same target material, the user needs to duplicate the data of this material in the input data file (copy and paste), assign the duplicate data set a different material name, and then use one material name for the target and the other material name for the other system components. Finally, EGSnrc uses restricted stopping powers rather than total cross sections to calculate the range of charged particles

in the enhanced medium. Because restricted stopping power is a separate input in the input data file, changing the total cross section does *not* affect the Range Rejection variance-reduction technique already implemented in EGSnrc (this is verified in the benchmarking section).

B. BCSE without UBS/DBS

The simplest case of BCSE implementation is when it is not combined with either UBS or DBS. In this case, and for a cross-section enhancement factor f_{enh} , when bremsstrahlung photons are produced in the enhanced medium, their weight W (typically unity) is reduced to W/f_{enh} to counteract the effect of cross-section enhancement. In addition, a uniform random number between 0 and 1 is sampled, and if it is larger than $1/f_{\text{enh}}$, the energy of the charged particle is kept at its value before the bremsstrahlung event took place; otherwise the energy of the charged particle is decremented by the amount of energy given to the bremsstrahlung photon. This means that the emission of a bremsstrahlung photons does not necessarily cause a reduction in the charged particle energy. This is done to avoid altering the physics of the charged particle transport in the enhanced medium.

Second-generation charged particles are created through photoelectric, Compton, and pair-production interactions of first-generation low-weight photons. This triggers higher generations of vanishingly low-weight photons and charged particles that, if tracked, will consume CPU time without contributing much to reducing the variance of the scored quantity. To avoid this, secondary charged particles are eliminated throughout the geometry by playing Russian Roulette with each of them with a survival probability of $1/f_{\text{enh}}$, and raising the weight of the surviving charged particles to the original weight W . This playing of Russian Roulette with secondary charged particles is given as an option to the user through the EGSnrc built-in flag `I_PLAY_RR`. All simulations in this study are done with the flag `ON`. We recommend playing Russian Roulette with secondary charged particles as long as photons (as opposed to charged particles) are the main focus of the simulation.

If *fat* photons (i.e., photons of large weight) reach the field of interest, they can compromise the statistics of the scored quantity. Fat photons of weight W are created through relaxation events after electron-impact ionization (both in the enhanced medium and elsewhere), through bremsstrahlung events outside the enhanced medium, and through positron annihilation events. To avoid this issue, every fat photon is *split* into f_{enh} photons, each with a reduced weight of W/f_{enh} . There should be no confusion between this splitting step, which is part of the BCSE algorithm to eliminate fat photons, and the standard UBS and DBS splitting techniques already used in the EGSnrc/BEAMnrc system. Finally, it should be noted that a possible alternative to splitting relaxation events after electron-impact ionization in the enhanced medium is to scale up the electron-impact ionization cross section in the enhanced medium by a factor f_{enh} and reduce the weight of the resulting relaxation photons to W/f_{enh} , but this is not implemented in this study.

When BCSE is not combined with UBS or DBS, and assuming Russian Roulette is played with secondary charged particles, the weight of all photons is W/f_{enh} and the weight of all charged particles is W .

C. BCSE with UBS/DBS

1. BCSE with UBS

To combine BCSE with a cross-section enhancement factor f_{enh} and UBS with a splitting number N_{split} , these steps are followed: (1) bremsstrahlung events in the enhanced medium are split N_{split} times and their weight is reduced from W to $W/(f_{\text{enh}}N_{\text{split}})$; (2) with a probability of $1/f_{\text{enh}}$, the energy of the charged particle is decremented by the amount of energy given to the bremsstrahlung photon; (3) any fat photon generated from any of the potential sources discussed in the previous section is split into $(f_{\text{enh}}N_{\text{split}})$ photons; and (4) if the user chooses to play Russian Roulette with secondary charged-particles, then it is played in the entire geometry with a survival probability of $1/(f_{\text{enh}}N_{\text{split}})$, otherwise it is turned off in the entire geometry for both BCSE and UBS. All simulations using combined BCSE and UBS in this study are done with the Russian Roulette flag ON.

When BCSE is combined with UBS, and assuming Russian Roulette is played with secondary charged-particles, the weight of all photons is $W/(f_{\text{enh}}N_{\text{split}})$ and the weight of all charged particles is W .

2. BCSE with DBS

To combine BCSE with a cross-section enhancement factor f_{enh} and DBS with a splitting number N_{split} without disturbing the complicated algorithm of DBS, the splitting number is made equal to N_{split} only when a bremsstrahlung event is about to take place in the enhanced medium and reset to $(f_{\text{enh}}N_{\text{split}})$ for all other aspects of the DBS algorithm. This ensures that fat particles and higher-generation particles are handled according to the original DBS algorithm. Only two extra actions are taken after a bremsstrahlung event in the enhanced medium takes place: (1) with a probability of $1/f_{\text{enh}}$, the energy of the charged particle is decremented by the amount of energy given to the bremsstrahlung photon and (2) if the weight of the bremsstrahlung photon generated in the enhanced medium is W/N_{split} , then it is reduced to $W/(f_{\text{enh}}N_{\text{split}})$; however, if its weight is W (fat photons are an integral part of the DBS algorithm²³), then Russian Roulette is played with the fat photon with a survival probability of $1/f_{\text{enh}}$. This is not to be confused with the built-in Russian Roulette in DBS, which creates the fat photon in the first place. This extra Russian Roulette step is necessary to prevent weight-variation issues within the field of interest, and it does *not* make the fat-photon issue (which is inherent to DBS) any better or worse than it is in the original DBS algorithm. Finally, DBS has the option to split charged particles beyond a user-specified plane. This option is still available if the user combines BCSE with DBS, where gains in both photon and electron scoring efficiency can be achieved.

When BCSE is combined with DBS, the weight of all photons reaching the field of interest is $W/(f_{\text{enh}}N_{\text{split}})$.

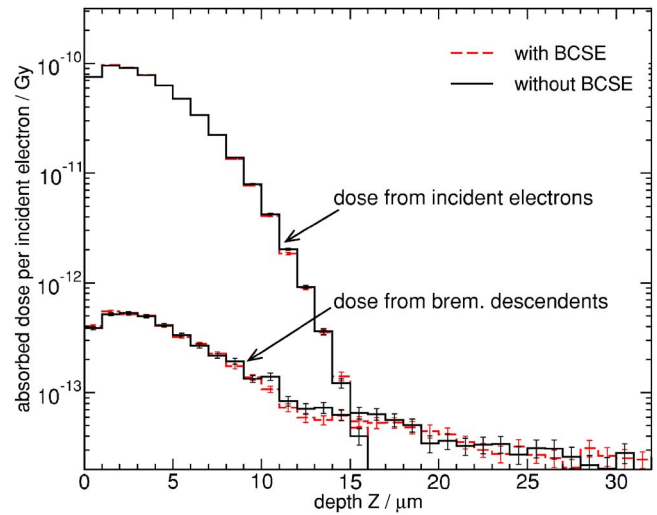


Fig. 2. Depth-dose distribution for 130 keV pencil beam of electrons normally incident on a tungsten slab. Dose is scored inside the slab around the central axis in small cylinders of 5 mm radius and 1 μm height each. Dose is split into two components: a component from direct energy deposition by the incident electrons, and a component from energy deposition by the charged particles descending from bremsstrahlung photons generated within the slab.

III. BENCHMARKING BCSE

BCSE is a true variance-reduction technique; if it is implemented properly, it should not bias any scored quantity.²⁷ To ensure its proper implementation, rigorous benchmarking tests are performed on all the various simulations outlined in the next section before they are used to study the performance of the BCSE technique. Other cases are also benchmarked to test particular issues. Examples of benchmarking tests performed are: (1) comparing simulation results with and without BCSE when using range rejection; (2) comparing depth-dose distributions inside the target material with and without BCSE for electrons incident on a tungsten slab; (3) repeating test 2 but for a 6 MeV monoenergetic positron-beam; (4) comparing simulation results with BCSE alone, with UBS/DBS alone, with BCSE+UBS and with BCSE+DBS; simulations are done for the two cases of electron-impact ionization ON and OFF; (5) repeating test 4 but for a 6 MeV monoenergetic positron-beam; and (6) comparing simulation results with and without BCSE when using the full Koch-Motz bremsstrahlung angular-distribution formula²⁸ and also when using only the leading term of it (because the DBS algorithm differs accordingly²³). Parameters such as spectral distribution, fluence profiles (where the heel effect can be seen for angled targets), and three-dimensional (3D) dose maps are used for comparison.

Figure 2 shows the results of one of the most stringent tests performed (test 2 above). The graph confirms that the energy loss by the charged particles along their tracks is the same, within statistics, with and without BCSE. It also shows that the extra photons generated by enhancing the bremsstrahlung cross section are generated *everywhere* along the charged-particle track, not only closer to the surface, and that their energy and angular distribution is the same as it is with-

out BCSE. Similar agreement is obtained for all the benchmarking tests, within 0.5%, for energy spectra, fluence profiles, and dose maps. Passing such rigorous tests confirms that the BCSE technique is a true variance-reduction technique and that it has been implemented correctly into EGSnrc/BEAMnrc. It also shows that the BCSE technique is compatible with the other variance-reduction techniques in EGSnrc/BEAMnrc, including Range Rejection, UBS, and DBS. This allows us to move into studying the performance of the new technique.

IV. PERFORMANCE OF BCSE

In studying the performance of the BCSE technique, we put emphasis on typical situations encountered in the clinical use of bremsstrahlung targets, both in diagnostic x-ray imaging and in radiotherapy, in order for the reported efficiency gains to be of greatest practical use. Simulations are done using two EGSnrc user-codes: BrachyDose²⁰ and a customized version of BEAMnrc.⁵ BrachyDose scores dose by calculating the collision kerma using a track-length estimator of fluence, weighted by the mass energy-absorption coefficient. The customized BEAMnrc version allows for grid scoring within the field of interest and reports the sum of the variance for all the scoring zones within the grid, which is then used as a measure of the variance s^2 in Eq. (1) for efficiency calculations. The most accurate physics available in EGSnrc is included (binding effects in Compton scattering, relaxation cascades after atomic vacancy creation, electron-impact ionization,⁸ spin effects for electron elastic scattering, single-scattering boundary-crossing algorithm, and Rayleigh scattering). For kilovoltage simulations, electrons and photons are tracked down to 1 keV. Tabulations from NIST for photon cross sections⁹ and for differential bremsstrahlung cross sections^{10,11} are used. The option of using only the leading term of the Koch-Motz bremsstrahlung angular-distribution formula²⁸ is chosen. This is because when only the leading term is used, BEAMnrc can calculate in advance the probability of photon emission into the solid angle of interest and generates only such photons, which substantially improves the DBS efficiency.²³

A rejection plane is introduced with DBS to terminate the histories of fat photons if they interact in the air layer just above the scoring plane. This prevents correlated split photons from being created close to the scoring plane. For large splitting numbers, if these correlated photons are not eliminated, they can compromise the statistics of some of the scoring zones within the field of interest. Our Monte Carlo studies show that eliminating these fat photons has a negligible effect on fluence scoring in the kilovoltage range for typical field sizes of interest.

A. Performance of BCSE without UBS/DBS

Although BCSE is meant to be used in combination with UBS or DBS to boost their efficiency gains, it is instructive to study the behavior of simulation efficiency versus f_{enh} without UBS/DBS. The diagnostic x-ray tube described in Sec. IV C below is used for that purpose. Four scoring grids

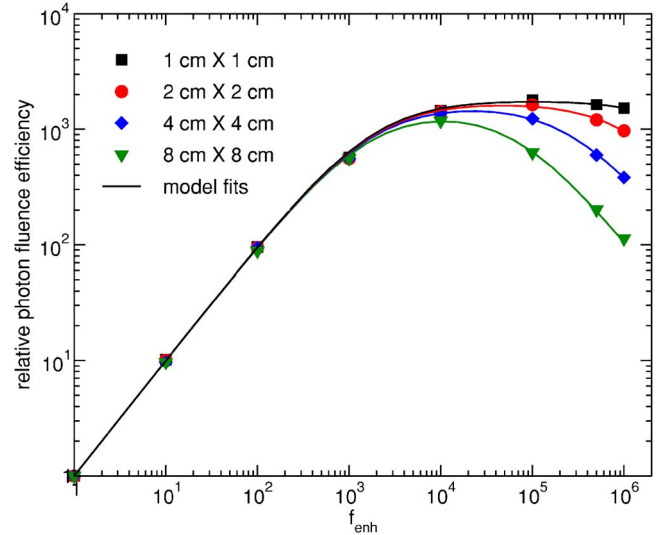


FIG. 3. The ratio of photon-fluence efficiency of a simulation with BCSE over the photon-fluence efficiency of the same simulation without BCSE, as a function of the cross-section enhancement factor (f_{enh}) for the 130 kV DC diagnostic tube described in Sec. IV C. Results are shown for four grids of square scoring zones in a 40×40 cm² field at 100 cm SSD. For efficiency calculations, the sum of the variance for all the scoring zones within each grid is used. The relative-efficiency behavior can be interpreted using Kawrakow's model (Refs. 24 and 26) (solid lines). The model can also be used to predict $f_{\text{enh}}^{\text{opt}}$ for largest efficiency gains when BCSE is used alone ($f_{\text{enh}}^{\text{opt}} = 104\,073, 46\,836, 22\,154, \text{ and } 10\,582$ for scoring-zone sizes $A = 1 \times 1, 2 \times 2, 4 \times 4, \text{ and } 8 \times 8$ cm², respectively). $f_{\text{enh}}^{\text{opt}}$ varies with the scoring-zone size roughly as $1/\sqrt{A}$.

are used for a 40×40 cm² field at 100 cm SSD; each grid has equal square scoring zones ($1 \times 1, 2 \times 2, 4 \times 4, \text{ and } 8 \times 8$ cm²). The cross-section enhancement factor f_{enh} is varied between 1 (no cross-section enhancement) and 1 000 000. Figure 3 shows the variation of the relative photon-fluence efficiency with f_{enh} . It can be seen that the numerical value of the relative efficiency is almost equal to the numerical value of f_{enh} in the range 1–1000, independent of the scoring-zone size. This can be explained as follows: For very small f_{enh} , less than one photon is emitted per incident electron, and so all photons fully contribute to reducing the variance in the scoring zones they fall into. As f_{enh} gets relatively larger (100–1000), more than one photon can be generated from the same incident electron; however, because there are still not too many photons generated from the same incident electron, they, on average, still fall into different scoring zones and fully contribute to reducing the variance in these zones, regardless of the scoring-zone size. This means that the effect of cross-section enhancement in this range is equivalent to increasing the number of histories, and since efficiency varies linearly with the number of histories, it also does so with f_{enh} in that range, as seen in Fig. 3. As f_{enh} gets much larger (>1000), many more than one photon is generated per incident electron. Such photons start falling in the same scoring zones and they do not contribute as much to reducing the variance because of the increased relative correlation between them,²⁵ yet they still consume the same CPU time to be tracked in the target. Thus, according to Eq. (1), the relative efficiency saturates and then drops. The big-

ger the scoring-zone size, the more chance photons generated from the same incident electron fall into a given scoring zone. This causes the peaks of relative photon-fluence efficiency for bigger scoring zones to be smaller in magnitude and at smaller f_{enh} values compared to the peaks of smaller scoring-zones, as seen in Fig. 3.

The efficiency behavior shown in Fig. 3 can also be explained in light of a recent theoretical model derived by Kawrakow.²⁶ The model was derived for UBS/DBS to explain the functional form of the relative photon-fluence efficiency versus the splitting number, and to predict the optimum splitting number. By replacing N_{split} in the derivation with f_{enh} , the derivation becomes applicable to the BCSE technique. A practical implementation of the derivation for UBS/DBS has recently been published.²⁴ Figure 3 shows the results of using that implementation for BCSE (with f_{enh} replacing N_{split}). The perfect agreement shows that the efficiency behavior when using the BCSE technique can be described theoretically using Kawrakow’s model. The model can also be used to predict the optimum f_{enh} for largest efficiency gain without need for exhaustive runs; this is useful if BCSE is used without UBS or DBS.

B. Performance of BCSE in 4π geometry (brachytherapy)

The largest efficiency gains over the current state-of-the-art of the EGSnrc system are expected when BCSE is combined with UBS for 4π-geometry simulations with low incident charged-particle energy. This expectation is because UBS is the only currently-available variance-reduction technique in the EGSnrc system for 4π-geometry simulations. The reported UBS efficiency gains are not that large on their own, and so BCSE will boost such gains, particularly at low energies where bremsstrahlung production is very rare.

An example of this situation is the calculation of the 3D dose distribution from the Xoft Axxent™ source, a miniature brachytherapy electronic x-ray source developed by Xoft.²⁹ The source consists of an electron gun in an evacuated tube with a thin coating of target material on a conically-shaped anode surface. The source operates between 40 and 50 kV DC. The geometry is modeled using Yegin’s general-purpose geometry package³⁰ for EGSnrc, and the simulation is done using BrachyDose.²⁰ Analog simulations of the source inside a 30×30×30 cm³ water phantom show that more than 95% of the simulation time is spent in generating the photons from the source, as opposed to tracking them in the water phantom. This reflects the importance of boosting the efficiency of the process of photon generation. For efficiency calculations, a cube of dimensions 1×1×1 cm³, with the x-ray source at its center, is divided into equal-size small voxels with dimensions relevant to clinical practice and to TG-43 dosimetry-parameter calculations²⁰ (0.3×0.3×0.3 mm³, 1.0×1.0×1.0 mm³, and 2.5×2.5×2.5 mm³). Dose uncertainty is averaged for the voxels making the faces of the 1×1×1 cm³ cube. Figure 4 shows, for an operating voltage of 50 kV DC, the relative dose-scoring efficiency for three voxel sizes, both when BCSE is used alone and when

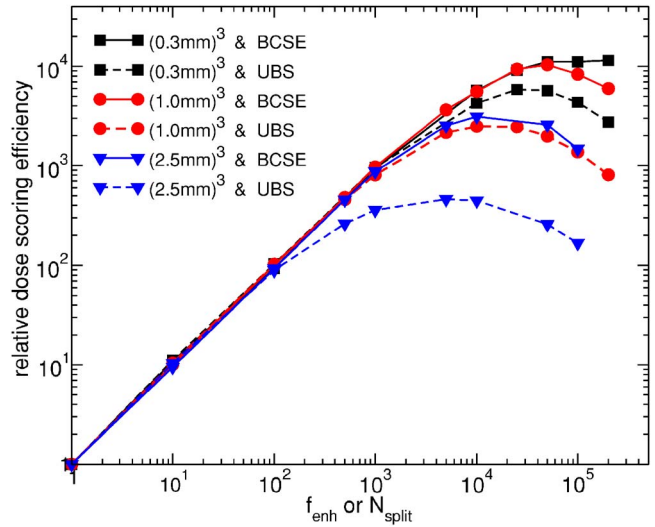


FIG. 4. The ratio of dose-scoring efficiency of a simulation with BCSE or with UBS over the dose-scoring efficiency of the same simulation without BCSE or UBS, as a function of the cross-section enhancement factor (f_{enh}) or the splitting number (N_{split}) for the Xoft Axxent™ (Ref. 29) 50 kV DC brachytherapy electronic x-ray source (an example of a 4π-geometry simulation). For efficiency calculations, dose uncertainty is averaged for the voxels making the faces of a cube of dimensions 1×1×1 cm³ around the x-ray source. The voxel sizes tested are: 0.3×0.3×0.3 mm³, 1.0×1.0×1.0 mm³, and 2.5×2.5×2.5 mm³. BCSE alone outperforms UBS. Further appreciable efficiency gains are achieved when BCSE is combined with UBS for the same simulations (see Table I).

UBS is used alone. Because BCSE creates photons with less correlation than UBS, it allows for a larger f_{enh} value before efficiency saturation (compared to the corresponding peak N_{split} value). BCSE also produces a higher-peak efficiency.

To combine BCSE with UBS, f_{enh} values of 50, 100, 500, 1000, and 2000 are tested, and each of them is combined with a wide range of N_{split} values. Table I summarizes the results for the three voxel sizes investigated. With the parameters as defined in the table caption, the following observations can be made:

TABLE I. Efficiency gains when optimally combining BCSE with UBS for the Xoft Axxent (Ref. 29) 50 kV DC brachytherapy electronic x-ray source (an example of a 4π-geometry simulation). $f_{\text{enh,ONLY}}^{\text{opt}}$ is the optimum cross-section enhancement factor when only BCSE is used. $N_{\text{split,ONLY}}^{\text{opt}}$ is the optimum splitting number when only UBS is used. $(f_{\text{enh}}^{\text{opt}}, N_{\text{split}}^{\text{opt}})$ is the optimum combination of cross-section enhancement with splitting. ϵ_{opt} is the ratio of efficiency when optimally combining BCSE with UBS over the efficiency without BCSE or UBS. R_{BCSE} is the ratio of efficiency when optimally combining BCSE with UBS over the peak efficiency when BCSE is used alone. R_U is the ratio of efficiency when optimally combining BCSE with UBS over the peak efficiency when UBS is used alone.

Side of cubic voxel (mm)	$f_{\text{enh,ONLY}}^{\text{opt}}$	$N_{\text{split,ONLY}}^{\text{opt}}$	$(f_{\text{enh}}^{\text{opt}}, N_{\text{split}}^{\text{opt}})$	ϵ_{opt}	R_{BCSE}	R_U
0.3	200 000	25 000	(500, 200)	13 032	1.13	2.22
1.0	50 000	10 000	(500, 100)	14 750	1.42	6.43
2.5	10 000	5 000	(1000, 50)	4 510	1.44	9.81

- The optimum combination ($f_{\text{enh}}^{\text{opt}}, N_{\text{split}}^{\text{opt}}$) yields efficiencies that are up to four orders of magnitude larger than those obtained with analog simulations, and up to a full order of magnitude larger than the corresponding peak efficiencies with UBS alone.
- When BCSE is combined with UBS, $f_{\text{enh}}^{\text{opt}}$ is not very sensitive to voxel-size change because $f_{\text{enh}}^{\text{opt}}$ does not get very large.
- R_U (the efficiency improvement relative to that of UBS alone) is much larger than R_{BCSE} (the efficiency improvement relative to that of BCSE alone). This means that most of the variance reduction is achieved through the cross-section enhancement rather than through the splitting.
- For a given source energy, R_U is larger for bigger scoring voxels because the advantage of cross-section enhancement over splitting in creating less-correlated photons is more prominent.

C. Performance of BCSE with diagnostic, mammography, and orthovoltage tubes

For directional geometry (as opposed to 4π geometry), the largest efficiency gains are expected when BCSE is optimally combined with DBS, with larger gains for lower incident charged-particle energies. This expectation is because DBS is the best splitting option for small solid-angle simulations. BCSE will then boost DBS efficiency gains by reducing the correlation between scored particles, especially at lower incident charged-particle energies.

To quantify BCSE performance in directional-geometry simulations, diagnostic, mammography, and orthovoltage tubes are simulated using BEAMnrc.⁵ The diagnostic tube specifications are: a 20° tungsten target in vacuum with copper backing, a beryllium window, aluminum added filtration, lead collimators, and a pair of heavy-metal jaws to shape rectangular fields. Simulation parameters are: $20 \times 20 \text{ cm}^2$ and $40 \times 40 \text{ cm}^2$ fields at 100 cm SSD and grid scoring-zone sizes of $1 \times 1 \text{ cm}^2$, $2 \times 2 \text{ cm}^2$, and $4 \times 4 \text{ cm}^2$. The tube operates at 130 kV DC. For the mammography tube, the differences from the diagnostic one are: a molybdenum target, molybdenum added-filtration, an $18 \times 18 \text{ cm}^2$ field at 65 cm SSD, and a grid scoring-zone size of $1.5 \times 1.5 \text{ cm}^2$. The tube operates at 20 kV DC. The orthovoltage tube specifications and simulation parameters are similar to those of the Siemens Stabilipan2 TH300 unit reported by Verhaegen *et al.*¹³ This includes: a 24° tungsten target, aluminum filtration, a close-ended lead-lined applicator with a 3 mm thick polymethylmethacrylate (PMMA) endplate, a $10 \times 10 \text{ cm}^2$ field at 52 cm SSD, and a grid scoring-zone size of $1 \times 1 \text{ cm}^2$. The tube operates at 230 kV DC. Exact specifications of the tubes simulated are not given here because these tubes are meant to be only representatives of different classes of x-ray generators.

Simulations with BCSE alone, with UBS alone, and with DBS alone are done first, and the corresponding relative photon-fluence efficiency curves are plotted. As expected,

DBS at its peak outperforms both BCSE and UBS at their peaks by about an order of magnitude, simply because of the directional nature of the DBS algorithm.

To combine BCSE with UBS/DBS, f_{enh} values of 10, 50, 100, 200, 300, 400, 500, and 1000 are tested, and each of them is combined with a wide range of N_{split} values for both UBS and DBS. Table II summarizes the results for all the investigated tube configurations, source energies, field sizes, and grid scoring-zone sizes. With the parameters as defined in the table caption, the following observations can be made:

- The optimum combination ($f_{\text{enh}}^{\text{opt}}, N_{\text{split}}^{\text{opt}}$) yields efficiencies that are up to five orders of magnitude larger than those obtained with analog simulations, and up to 4.8 times larger than the corresponding peak efficiencies with DBS alone.
- For a given tube and source energy, when BCSE is combined with UBS/DBS, $f_{\text{enh}}^{\text{opt}}$ is not very sensitive to field-size change or to scoring-zone size change.
- $f_{\text{enh}}^{\text{opt}}$ increases as the source energy decreases (130 to 20 keV) and as the target material changes to a lower-Z material that produces less bremsstrahlung (tungsten to molybdenum).
- For a given tube, source energy and field size, $f_{\text{enh_ONLY}}^{\text{opt}}$, and $N_{\text{split_ONLY}}^{\text{opt}}$, and $N_{\text{split}}^{\text{opt}}$ all have a $1/\sqrt{A}$ dependence on the size of the grid scoring zone (A).
- For a given tube, source energy, field size, and grid scoring-zone size, R_D (the efficiency improvement relative to that of DBS alone) is consistently larger than R_U (the efficiency improvement relative to that of UBS alone). This is because, when BCSE is combined with DBS, all the extra photons generated due to the cross-section enhancement contribute to the scored quantity (because the ones directed away from the field are not generated except for one fat photon representing them), whereas when BCSE is combined with UBS, all the extra photons are generated and tracked, and only a fraction of them contributes to the scored quantity.
- For a given tube, source energy, and grid scoring-zone size, R_D is consistently larger for smaller field-sizes ($20 \times 20 \text{ cm}^2$) than it is for larger ones ($40 \times 40 \text{ cm}^2$). This is because as the field size gets smaller, the optimum splitting number with DBS alone increases as \sqrt{A} but the actual number of photons going towards the field of interest (and thus sampled) decreases roughly as $1/A$, so the net effect is a reduction in the number of sampled photons by $1/\sqrt{A}$. This implies that the fractional time spent in tracking the charged particles gets larger, and so the effect of cross-section enhancement becomes more obvious.
- For a given tube, source energy, and field size, both R_U and R_D get larger as the grid scoring-zone size gets larger (for the same reason discussed before for the voxel-size effect in 4π geometry).

TABLE II. Efficiency gains when optimally combining BCSE with UBS/DBS for the diagnostic, mammography and orthovoltage tubes described in Sec. IV C. Parameters are defined as in the caption of Table I, except that $N_{\text{split_ONLY}}^{\text{opt}}$ and ϵ_{opt} refer here to either UBS or DBS. In addition, R_D is the ratio of efficiency when optimally combining BCSE with DBS over the peak efficiency when DBS is used alone.

Field size (cm ²)	Scoring zone size (cm ²)	UBS or DBS				R_U (UBS) or R_D (DBS)	
		$f_{\text{enh_ONLY}}^{\text{opt}}$	DBS	$N_{\text{split_ONLY}}^{\text{opt}}$	$(f_{\text{enh}}^{\text{opt}}, N_{\text{split}}^{\text{opt}})$	ϵ_{opt}	
Diagnostic tube, 130 kV DC, 100 cm SSD							
20×20	1×1	100 000		50 000	(100, 2500)	4 137	1.19
	2×2	50 000	UBS	25 000	(200, 500)	3 831	1.38
	4×4	25 000		10 000	(200, 200)	3 179	1.62
	1×1			200 000	(200, 2000)	84 450	1.74
	2×2		DBS	100 000	(200, 1000)	54 874	2.22
	4×4			50 000	(200, 500)	30 181	3.37
	1×1	100 000		50 000	(100, 2500)	3 816	1.21
	2×2	50 000	UBS	25 000	(200, 500)	3 886	1.42
	4×4	25 000		10 000	(200, 200)	3 575	1.68
40×40	1×1			100 000	(100, 2000)	40 766	1.37
	2×2		DBS	50 000	(200, 1000)	35 382	1.92
	4×4			25 000	(200, 500)	20 222	2.57
Mammography tube, 20 kV DC, 65 cm SSD							
18×18	1.5×1.5	500 000	UBS	50 000	(500, 1000)	14 512	1.75
			DBS	500 000	(500, 2000)	251 240	4.80
Orthovoltage tube, 230 kV DC, 52 cm SSD							
10×10	1×1	100 000	DBS	100 000	(100, 2000)	83 511	2.10

- For a given tube, source energy, and grid scoring-zone size, R_U and $f_{\text{enh_ONLY}}^{\text{opt}}$ do not change with the field size (20×20 cm² or 40×40 cm²). This is because, unlike DBS, both UBS and BCSE are non-directional, and all the photons are generated and tracked regardless of the size of the field of interest.
- Both R_U and R_D increase as the source energy decreases. This is because the bremsstrahlung-emission process is rarer, which makes the advantage of combining BCSE with splitting more prominent.

Although combining BCSE with UBS boosts the overall efficiency, DBS efficiencies with and without BCSE remain much higher than those for UBS. This suggests that combining BCSE with DBS is the optimum choice for directional geometries.

D. Performance of BCSE with clinical linear accelerators

For monoenergetic electrons of kinetic energy 6 MeV, incident on a 1 mm tungsten slab followed by a 1.5 mm copper slab (a typical transmission-type target arrangement), our analog Monte Carlo studies show that although about 3.8 bremsstrahlung photons are emitted per incident charged particle, only about 18% of those bremsstrahlung photons survive target self-attenuation and make it out of the target towards the patient plane. In other words, only $3.8 \times 0.18 = 0.7$ photons per incident charged particle make it out of the

target towards the patient plane. This gives potential for efficiency improvements when BCSE is combined with DBS in the megavoltage range as well.

To quantify BCSE performance in the megavoltage range, 6 and 18 MV Varian accelerators with 10×10 cm² fields at 100 cm SSD are simulated. Simulation parameters are similar to those used by Sheikh-Bagheri and Rogers.³¹ Two grids within the 10×10 cm² field are investigated: a grid of equal 1×1 cm² scoring zones and a grid of one big 10×10 cm² scoring zone. Simulations with DBS alone are done first and the peak efficiency is determined. To combine BCSE with DBS, f_{enh} values of 2, 5, 10, 20, 30, 50, and 100 are tested, and each of them is combined with a wide range of N_{split} values for DBS. Table III summarizes the results for the 6

TABLE III. Efficiency gains when optimally combining BCSE with DBS for the 6 and 18 MV Varian accelerators (Ref. 31) with 10×10 cm² fields at 100 cm SSD. Parameters are defined as in the caption of Tables I and II, except that $N_{\text{split_ONLY}}^{\text{opt}}$ and ϵ_{opt} refer here to only DBS.

Beam quality (MV)	Scoring-zone size (cm ²)	$f_{\text{enh_ONLY}}^{\text{opt}}$	$N_{\text{split_ONLY}}^{\text{opt}}$	$(f_{\text{enh}}^{\text{opt}}, N_{\text{split}}^{\text{opt}})$	ϵ_{opt}	R_D
6	1×1	4500	3500	(20, 750)	823	1.43
	10×10	200	250	(20, 50)	125	2.62
18	1×1	800	500	(20, 100)	83	1.21

and 18 MV beams. With the parameters as defined in the table caption, it can be seen that even in the megavoltage range with grid scoring-zone sizes of clinical relevance, the optimum combination ($f_{\text{enh}}^{\text{opt}}, N_{\text{split}}^{\text{opt}}$) yields efficiencies that are up to 800 times larger than those obtained with analog simulations, and up to 40% larger than the corresponding peak efficiencies with DBS alone. In addition, for the 6 MV beam, when the whole $10 \times 10 \text{ cm}^2$ field is considered as one big scoring zone, the efficiency gain is a factor of 2.6 over that with optimum DBS alone.

V. DISCUSSION

When combining BCSE with UBS/DBS, the goal is to find the optimum combination ($f_{\text{enh}}^{\text{opt}}, N_{\text{split}}^{\text{opt}}$) that achieves the maximum efficiency gain for the simulation. Using cross-section enhancement creates uncorrelated photons but takes a little more CPU time per photon than splitting. Using splitting creates correlated photons but takes a little less CPU time per photon than cross-section enhancement. One would then expect that the optimum combination is to use a cross-section enhancement factor $f_{\text{enh}}^{\text{ONE}}$ that produces *exactly one* bremsstrahlung photon per incident charged particle (to get as many uncorrelated photons as possible), and then do the rest of the variance reduction through splitting (to save CPU time). Figure 1 can be used to estimate this $f_{\text{enh}}^{\text{ONE}}$. For example, for 50 keV monoenergetic electrons incident on a tungsten target (the brachytherapy x-ray source), the probability of emission of one bremsstrahlung photon per incident charged-particle is 0.024, and so $f_{\text{enh}}^{\text{ONE}} = 1/0.024 \approx 42$. Similarly, $f_{\text{enh}}^{\text{ONE}} \approx 250$ for 20 keV electrons incident on a molybdenum target (the mammography tube), ~ 12 for 130 keV electrons incident on a tungsten target (the diagnostic tube), and ~ 9 for 230 keV electrons incident on a tungsten target (the orthovoltage tube). However, if a cross-section enhancement factor of only $f_{\text{enh}}^{\text{ONE}}$ is used, self-attenuation in the target material, the tube exit window, and the added filtration eliminates many of these uncorrelated bremsstrahlung photons and brings the average number of bremsstrahlung photons exiting the target per incident charged particle to less than unity. In the diagnostic tube described in Sec. IV C, only 10% of the bremsstrahlung photons generated inside the target survive the self-attenuation. This observation suggests that using a cross-section enhancement factor $f_{\text{enh}} > f_{\text{enh}}^{\text{ONE}}$ to recreate the uncorrelated photons that do not survive self-attenuation will still have an advantage over splitting, as long as the time penalty is not too large.

In simulations involving bremsstrahlung targets, most of the simulation time is spent in tracking the charged particles as opposed to generating the bremsstrahlung photons. This implies that the fractional increase in CPU time-per-history for generating the bremsstrahlung photons through cross-section enhancement rather than through splitting is negligible for small f_{enh} values; it becomes appreciable only when f_{enh} gets large, as seen in Fig. 5. The trend in the figure explains why $f_{\text{enh}}^{\text{opt}}$ values shown in Tables I and II are larger than the corresponding $f_{\text{enh}}^{\text{ONE}}$ values estimated above. It also

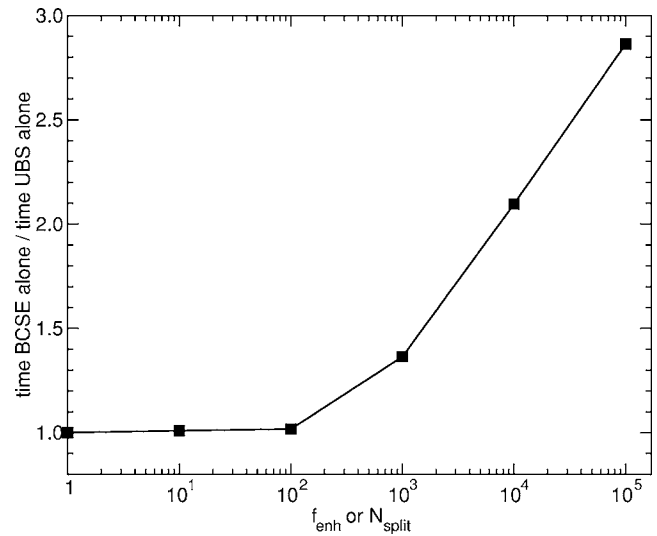


FIG. 5. The ratio of time-per-history when using BCSE alone with a cross-section enhancement factor f_{enh} over the time-per-history when using UBS alone with a splitting number N_{split} , as a function of the cross-section enhancement factor (f_{enh}) or the splitting number (N_{split}) for the 130 kV DC diagnostic-tube described in Sec. IV C. The flat behavior at small f_{enh} and N_{split} values is because most of the time is spent in tracking the electrons, which implies that generating the photons through cross-section enhancement versus splitting does not change the overall time-per-history. The linear behavior at large f_{enh} and N_{split} values is because most of the time is spent in producing and tracking the photons, which implies that generating the photons through cross-section enhancement versus splitting becomes the overriding factor in determining the time-per-history.

suggests that the optimum use of combined BCSE and splitting is to use BCSE for as long as the time penalty is less than the gain in the variance reduction; afterwards, complementary splitting should be used.

Figure 6 shows an example of the efficiency-gain behavior while searching for the optimum combination ($f_{\text{enh}}^{\text{opt}}, N_{\text{split}}^{\text{opt}}$). Although the scope of the study is the kilovoltage range, the 6 MV accelerator is chosen because in the megavoltage range, efficiency gains are more sensitive to slight variations in f_{enh} and N_{split} , which serves better in illustrating the efficiency-gain behavior. It can be seen that many different ($f_{\text{enh}}, N_{\text{split}}$) pairs can achieve comparable efficiency gains, although the pair (20, 750) gives the maximum. The magnitude of the peak-efficiency gains is smaller for very small f_{enh} (5, for example), increases to a maximum ($f_{\text{enh}}=20$), and then drops again for larger f_{enh} (50, for example) when the time penalty is more than the variance reduction that the cross-section enhancement gives over the splitting.

Based on the observations above, the following two steps are proposed for optimizing production runs that involve bremsstrahlung targets:

Step 1: The user chooses an optimum cross-section enhancement factor depending on the simulation type. Recommended $f_{\text{enh}}^{\text{opt}}$ are summarized in Table IV. Getting the maximum efficiency gain is not very sensitive to the exact choice of $f_{\text{enh}}^{\text{opt}}$. In addition, $f_{\text{enh}}^{\text{opt}}$ itself is not very sensitive to tube configuration, to scoring-zone size, or to voxel size, and so the proposed numbers should suffice and the complementary

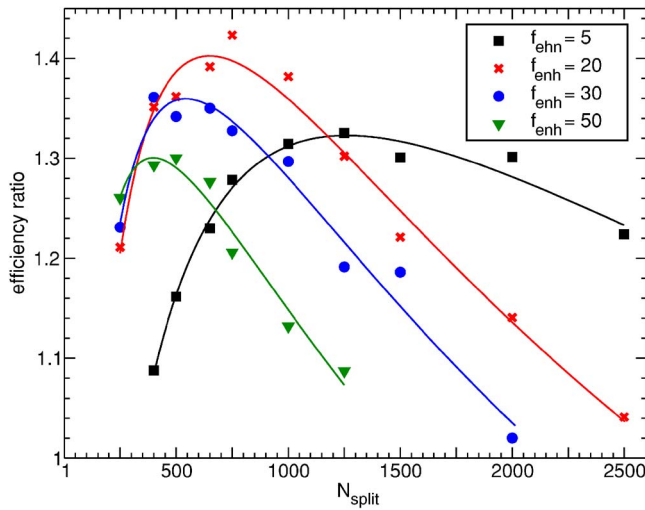


FIG. 6. The ratio of photon-fluence efficiency when BCSE and DBS are combined over the peak efficiency when DBS is used alone, as a function of both the cross-section enhancement factor (f_{enh}) and the splitting number (N_{split}) for the 6 MV Varian accelerator (Ref. 31). A $10 \times 10 \text{ cm}^2$ field at 100 cm SSD is split into equal square scoring zones of $1 \times 1 \text{ cm}^2$. Efficiency gains for simulations with lower f_{enh} values peak at larger N_{split} values. From Kawrakow's model (Refs. 24 and 26) (solid lines), the $(f_{\text{enh}}, N_{\text{split}})$ pairs of (5, 1263), (20, 651), (30, 544), and (50, 399) give the four peaks in the graph.

$N_{\text{split}}^{\text{opt}}$ should pick up any little difference and get the efficiency gain very close to its maximum.

Step 2: The user determines the optimum $N_{\text{split}}^{\text{opt}}$ (this applies to both UBS and DBS) by applying Kawrakow's model^{24,26} as follows:

- perform a few short runs with $f_{\text{enh}}^{\text{opt}}$ from step 1 combined with a number of N_{split} values, and calculate the efficiency $\varepsilon_{N_{\text{split}}}$ for each run;
- fit $N_{\text{split}}/\varepsilon_{N_{\text{split}}}$ versus $(N_{\text{split}}-1)$ to the following quadratic equation:

$$\frac{N_{\text{split}}}{\varepsilon_{N_{\text{split}}}} = A_0 + A_1(N_{\text{split}} - 1) + A_2(N_{\text{split}} - 1)^2 \quad (4)$$

where $A_i, i=0, 1, 2$ are the polynomial coefficients;

- calculate $N_{\text{split}}^{\text{opt}}$ using $N_{\text{split}}^{\text{opt}} = \sqrt{A_0/A_2}$.

TABLE IV. Recommended optimum cross-section enhancement factors ($f_{\text{enh}}^{\text{opt}}$) when combining BCSE with splitting techniques, for typical situations in diagnostic x-ray imaging and in radiotherapy that involve bremsstrahlung targets.

Simulation type	Incident electron energy range	Recommended $f_{\text{enh}}^{\text{opt}}$
4π geometry (brachytherapy)	Kilovoltage range	500
X-ray tubes	Mammography range	500
X-ray tubes	Diagnostic range	200
X-ray tubes	Orthovoltage range	100
Clinical linear accelerators	Megavoltage range	20

TABLE V. CPU time $T(2\%)$ required to reach an average of 2% uncertainty on the fluence when an optimized EGSnrc/BEAMnrc system is used to simulate realistic radiotherapy and diagnostic machines. Simulations are done on a single 3.0 GHz Intel[®]-Woodcrest processor using a g77 compiler.

Simulation case	SSD (cm)	Field size (cm ²)	Scoring-zone size (cm ²)	$T(2\%)$ (s)
130 kV DC diagnostic tube	100	20×20	1×1	100
			2×2	56
			4×4	21
	100	40×40	1×1	146
			2×2	85
20 kV DC mammography tube	65	18×18	1.5×1.5	43
230 kV DC orthovoltage tube	52	10×10	1×1	37
6 MV Varian-accelerator	100	10×10	1×1	20
			10×10	1.4
18 MV Varian accelerator	100	10×10	1×1	56

Production runs then use the cross-section enhancement factor $f_{\text{enh}}^{\text{opt}}$ from step 1 and the splitting number of $N_{\text{split}}^{\text{opt}}$ from step 2 for maximum simulation-efficiency.

For fluence profiles, when the EGSnrc/BEAMnrc system is optimized as explained above, it usually takes about one minute on a single 3.0 GHz Intel[®]-Woodcrest processor to simulate realistic radiotherapy or diagnostic machines to an average uncertainty of 2% on photon fluence. Table V shows the timing results for various situations of clinical interest. For spectral distributions, when the optimum combination of f_{enh} and N_{split} for fluence scoring is used to obtain the spectral distribution, a 1-min simulation on the same processor

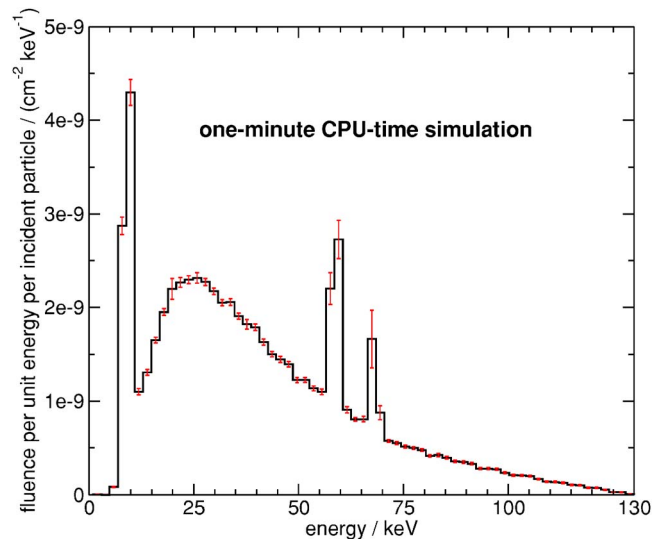


FIG. 7. A 1 min simulation to obtain the spectral distribution for the unfiltered 130 kV DC diagnostic tube described in Sec. IV C. The graph shows the average spectrum over a $20 \times 20 \text{ cm}^2$ field at 100 cm SSD in 2 keV energy bins. The optimum combination of f_{enh} and N_{split} for fluence scoring is used. The simulation is done on a single 3.0 GHz Intel[®]-Woodcrest processor using a g77 compiler.

yields reasonably-good statistics, as shown in Fig. 7. In the figure, large L-lines can be seen because of lack of filtration and because of the relatively larger bin width (which combines nearby L-peaks into a few large peaks). Uncertainty on the characteristic peaks is larger than it is on the bremsstrahlung spectrum. This is because all relaxation photons, which are the main contributor to the characteristic peaks, score in very few energy bins, so that the chance of correlated photons falling in the same energy bin is much higher than it is for the bremsstrahlung photons. Longer simulation times (\sim a few minutes) yield better and more uniform statistical fluctuations. In addition, if fluence profiles are used to get dose distribution in a phantom, the CPU time for transport in the phantom adds to the overall simulation time.

For the user to incorporate the BCSE technique into any EGSnrc user code (other than BEAMnrc), two macro calls need to be made: the first call is to adjust the cross sections (done after reading the input data file), and the second to make the BCSE technique unbiased (done in subroutine AUSGAB, see EGSnrc manual⁴). We intend to make the BCSE macros available as part of the standard EGSnrc macros. For BEAMnrc, incorporating BCSE requires hard coding in AUSGAB to combine BCSE with DBS. We intend to make the BCSE technique a standard option in future releases of BEAMnrc. Once the macros are part of the standard release of EGSnrc/BEAMnrc, the user will have the option, through the graphical user interface of the user code, to use BCSE. If the option is chosen, the user will be asked for three simple inputs: the medium in which to enhance the bremsstrahlung cross section, the enhancement factor, and whether or not to play Russian Roulette with secondary charged particles. All the details of the BCSE algorithm will be handled internally by the system.

VI. CONCLUSION

In this study, the bremsstrahlung cross-section enhancement variance-reduction technique is implemented and benchmarked in the EGSnrc/BEAMnrc system. Combining BCSE with the existing splitting techniques improves the simulation efficiency both in the kilovoltage and megavoltage range. Efficiency gains with optimum combinations of splitting and cross-section enhancement can be up to five orders of magnitude over those obtained with analog simulations, and up to a full order of magnitude over those obtained with optimized splitting alone (which is the state-of-the-art of the EGSnrc/BEAMnrc system before this study was carried out). For all EGSnrc/BEAMnrc simulations that involve bremsstrahlung targets, this study recommends (1) combining BCSE with the existing variance-reduction techniques, particularly UBS and DBS, (2) using the proposed optimum cross-section enhancement factors from Table IV for typical situations in diagnostic x-ray imaging and in radiotherapy, and (3) adopting the two-step algorithm outlined in Sec. V. for simulation optimization. The improvement this study adds to the EGSnrc/BEAMnrc system, along with other recent improvements, make the system ideally suitable

for more accurate and efficient simulations, and opens the door wider for more use of Monte Carlo in medical physics research and in clinical practice.

ACKNOWLEDGMENTS

The authors would like to thank Randy Taylor and Gultekin Yegin for help with BrachyDose, Blake Walters at NRC for grid scoring, Ernesto Mainegra-Hing at NRC for the rejection plane with DBS, Iwan Kawrakow at NRC, and the members of the Carleton Laboratory for Radiotherapy Physics (CLRP) for helpful comments on the manuscript. Some of the calculations in this study are done on WestGrid computing facilities. This work is partially funded by NSERC and The Canada Research Chairs program.

^a)Electronic mail: eali@physics.carleton.ca

^b)Electronic mail: drogers@physics.carleton.ca

WWW: <http://www.physics.carleton.ca/~drogers/>

¹M. Berger and S. Seltzer, "ETRAN Monte Carlo code system for electron and photon transport through extended media," Report CCC-107, Radiation Shielding Information Centre, ORNL, Oak Ridge, Tennessee, 1973.

²F. Salvat, J. M. Fernandez-Varea, J. Baro, and J. Sempau, "PENLOPE, a code system for Monte Carlo simulation of electron and photon transport," University of Barcelona Report, 2003.

³E. Acosta, X. Llovet, E. Coleoni, and J. Riveros, "Monte Carlo simulation of x-ray emission by kilovolt electron bombardment," *J. Appl. Phys.* **83**, 6038–6049 (1998).

⁴I. Kawrakow and D. W. O. Rogers, "The EGSnrc Code System: Monte Carlo simulation of electron and photon transport," Technical Report PIRS-701, National Research Council of Canada, Ottawa, Canada, 2006.

⁵D. W. O. Rogers, B. Walters, and I. Kawrakow, *BEAMnrc Users Manual*, NRC Report PIRS 509(a)revK (2006).

⁶R. L. Ford and W. R. Nelson, "The EGS code system—Version 3," Report SLAC-210, Stanford Linear Accelerator Center, Stanford, California, 1978.

⁷I. Kawrakow, "Accurate condensed history Monte Carlo simulation of electron transport," I. EGSnrc, the new EGS4 version, *Med. Phys.* **27**, 485–498 (2000).

⁸I. Kawrakow, "Electron impact ionization cross sections for EGSnrc," *Med. Phys.* **29**, 1230 (2002).

⁹M. J. Berger and J. H. Hubbell, "XCOM: Photon cross sections on a personal computer," Report NBSIR87-3597, NIST, Gaithersburg, MD20899, 1987.

¹⁰S. M. Seltzer and M. J. Berger, "Bremsstrahlung spectra from electron interactions with screened atomic nuclei and orbital electrons," *Nucl. Instrum. Methods Phys. Res. B* **12**, 95–134 (1985).

¹¹S. M. Seltzer and M. J. Berger, "Bremsstrahlung energy spectra from electrons with kinetic energy from 1 keV to 10 GeV incident on screened nuclei and orbital electrons of neutral atoms with $Z=1-100$," *At. Data Nucl. Data Tables* **35**, 345–418 (1986).

¹²L. Ben-Omrane, F. Verhaegen, N. Chahed, and S. Mtimet, "An investigation of entrance surface dose calculations for diagnostic radiology using Monte Carlo simulations and radiotherapy dosimetry formalisms," *Phys. Med. Biol.* **48**, 1809–1824 (2003).

¹³F. Verhaegen, A. E. Nahum, S. Van de Putte, and Y. Namito, "Monte Carlo modelling of radiotherapy kV x-ray units," *Phys. Med. Biol.* **44**, 1767–1789 (1999).

¹⁴M. Bhat, J. Pattison, G. Bibbo, and M. Caon, "Off-axis x-ray spectra: A comparison of Monte Carlo simulated and computed spectra with measured spectra," *Med. Phys.* **26**, 303–309 (1999).

¹⁵L. M. N. Tavora, E. J. Morton, F. P. Santos, and T. H. V. T. Dias, "Simulation of x-ray tubes for imaging applications," *IEEE Trans. Nucl. Sci.* **47**, 1493–1498 (2000).

¹⁶F. Verhaegen and I. A. Castellano, "Microdosimetric characterisation of 28 kVp MoMo RhRh RhAl WRh and MoRh mammography x-ray spectra," *Radiat. Prot. Dosim.* **99**, 393–396 (2002).

¹⁷F. Verhaegen, B. Reniers, F. Deblois, S. Devic, J. Seuntjens, and D. Hristov, "Dosimetric and microdosimetric study of contrast-enhanced radio-

- therapy with kilovolt x-rays," *Phys. Med. Biol.* **50**, 3555–3569 (2005).
- ¹⁸H. Deloar *et al.*, "Investigations of different kilovoltage x-ray energy for three-dimensional converging stereotactic radiotherapy system: Monte Carlo simulation with CT data," *Med. Phys.* **33**, 4635–4642 (2006).
- ¹⁹R. E. P. Taylor, G. Yegin, and D. W. O. Rogers, "Monte Carlo Modeling of the Xofig Axxent™ x-ray source," *Med. Phys.* **33**, 2205 (abs) (2006).
- ²⁰R. E. P. Taylor, G. Yegin, and D. W. O. Rogers, "Benchmarking BrachyDose: voxel-based EGSnrc Monte Carlo calculations of TG-43 dosimetry parameters," *Med. Phys.* **34**, 445–457 (2007).
- ²¹W. R. Nelson, H. Hirayama, and D. W. O. Rogers, "The EGS4 Code System," Report SLAC-265, Stanford Linear Accelerator Center, Stanford, California, 1985.
- ²²D. W. O. Rogers, B. A. Faddegon, G. X. Ding, C.-M. Ma, J. Wei, and T. R. Mackie, "BEAM: A Monte Carlo code to simulate radiotherapy treatment units," *Med. Phys.* **22**, 503–524 (1995).
- ²³I. Kawrakow, D. W. O. Rogers, and B. Walters, "Large efficiency improvements in BEAMnrc using directional bremsstrahlung splitting," *Med. Phys.* **31**, 2883–2898 (2004).
- ²⁴E. Mainegra-Hing and I. Kawrakow, "Efficient x-ray tube simulations," *Med. Phys.* **33**, 2683–2690 (2006).
- ²⁵B. R. B. Walters, I. Kawrakow, and D. W. O. Rogers, "History by history statistical estimators in the BEAM code system," *Med. Phys.* **29**, 2745–2752 (2002).
- ²⁶I. Kawrakow, "On the efficiency of photon beam treatment head calculations," *Med. Phys.* **32**, 2320–2326 (2005).
- ²⁷I. Lux and L. Koblinger, *Monte Carlo particle transport methods: neutron and photon calculations* (CRC Press, New York, 1991).
- ²⁸H. W. Koch and J. W. Motz, "Bremsstrahlung cross-section formulas and related data," *Rev. Mod. Phys.* **31**, 920–955 (1959).
- ²⁹M. J. Rivard, S. D. Davis, L. A. DeWerd, T. W. Rusch, and S. Axelrod, "Calculated and measured brachytherapy dosimetry parameters in water for the Xofig Axxent x-Ray source: An electronic brachytherapy source," *Med. Phys.* **33**, 4020–4032 (2006).
- ³⁰G. Yegin, "A new approach to geometry modelling of Monte Carlo particle transport: an application to EGS," *Nucl. Instrum. Methods Phys. Res. B* **211**, 331–338 (2003).
- ³¹D. Sheikh-Bagheri and D. W. O. Rogers, "Calculation of nine megavoltage photon beam spectra using the BEAM Monte Carlo code," *Med. Phys.* **29**, 391–402 (2002).